scientific reports

Check for updates

OPEN

# Comparative study on high-pressure physical properties of monoclinic $MgCO_3$ and $Mg_2CO_4$

Zi-Jiang Liu[1]✉, Tian Li[1], Xiao-Wei Sun[1], Cai-Rong Zhang[2] & Jia-Qi Ju[1]

**The physical properties of Mg-carbonate at high temperature and pressure are crucial for understanding the deep carbon cycle. Here, we use first-principles calculations to study the physical properties of $MgCO_3$-*C*2/*m* and $Mg_2CO_4$-*P*2$_1$/*c* under high pressure. The research shows that the structure and equation of state of $MgCO_3$-*C*2/*m* are in good agreement with the experimental results, and the phase transition pressure of $Mg_2CO_4$ from *pnma* to *P*2$_1$/*c* structure is 44.66 GPa. By comparing the elastic properties, seismic properties and anisotropy of $MgCO_3$-*C*2/*m* and $Mg_2CO_4$-*P*2$_1$/*c*, it is found that the elastic modulus and sound velocity of $Mg_2CO_4$-*P*2$_1$/*c* are smaller than those of $MgCO_3$-*C*2/*m*, while the anisotropy is larger than that of $MgCO_3$-*C*2/*m*. These results indicate that $Mg_2CO_4$-*P*2$_1$/*c* exists in the deep mantle and may be the main reason why carbonate cannot be detected. The minimum thermal conductivity of $MgCO_3$-*C*2/*m* and $Mg_2CO_4$-*P*2$_1$/*c* is the largest in the [010] direction and the smallest in the [001] direction. The thermodynamic properties of $MgCO_3$-*C*2/*m* and $Mg_2CO_4$-*P*2$_1$/*c* are predicted using the quasi-harmonic approximation (QHA) method.**

Magnesite (space group $R\bar{3}c$) is subducted into the deep mantle as the primary carbon carrier, and its high-temperature and high-pressure physical properties are critical for understanding the deep carbon cycle[1,2]. Previous studies have mainly focused on the structural phase transition of $MgCO_3$-$R\bar{3}c$ under high-temperature and high-pressure conditions, transforming to monoclinic $MgCO_3$ (space group *C*2/*m*) at around 80 GPa. Oganov et al. used the USPEX method to predict for the first time that $MgCO_3$-*C*2/*m* is most stable in the lower mantle greater than 82.4 GPa[3]. $MgCO_3$-*C*2/*m* has 30 atoms, in which adjacent oxygen atoms form tetrahedra around carbon atoms, and Mg atoms are in octet and tenfold coordination. Subsequently, the structure of $MgCO_3$-*C*2/*m* was verified experimentally[4–6] and theoretically[7–13]. Recently, Gavryushkin et al. used USPEX and AIRSS methods to find that $MgCO_3$ reacts with MgO to form $Mg_2CO_4$, which has two structures, orthorhombic (space group *Pnma*) and monoclinic (space group *P*2$_1$/*c*), and its structure is *P*2$_1$/*c* when the pressure is higher than 50 GPa[14]. Their experiments later confirmed the existence of $Mg_2CO_4$-*P*2$_1$/*c* at the temperature and pressure of the Earth's lower mantle[15]. $Mg_2CO_4$-*P*2$_1$/*c* has 28 atoms, it is isostructural to $\beta$-$Ca_2SiO_4$[16], and the atoms at the two positions Mg(1) and Mg(2) are six-coordinated, with octahedral coordination polyhedra. Earlier reports[17–20], although the structure of $Mg_2CO_4$ was not determined, believed that it is stable at high pressure.

To understand the carbon cycle in the deep earth, it is crucial to study the structure, phase transition, equations of state, elasticity, thermodynamics, and thermal conductivity of $MgCO_3$-*C*2/*m* and $Mg_2CO_4$-*P*2$_1$/*c* under high pressure. Recently, Maeda et al. measured the equation of state of $MgCO_3$-*C*2/*m* at high pressure[6]. Since it is extremely difficult to measure the elastic constants, thermodynamic parameters, and thermal conductivity of minerals experimentally, the properties of $MgCO_3$-*C*2/*m* and $Mg_2CO_4$-*P*2$_1$/*c* have not been reported experimentally. Even the elastic constant of $MgCO_3$-$R\bar{3}c$ can only be measured to 13.7 GPa[21], and its thermodynamic properties are only at low pressure, and the results at high pressure are extrapolated[22–24].

In the present work, the structures, phase transitions, equations of state, elastic properties, seismic properties, and minimum thermal conductivity of $MgCO_3$-*C*2/*m* and $Mg_2CO_4$-*P*2$_1$/*c* at high pressure are investigated using first-principles calculations and compared with the available experimental and theoretical results. The QHA method is adopted to research the thermodynamic properties of $MgCO_3$-*C*2/*m* and $Mg_2CO_4$-*P*2$_1$/*c*.

[1]School of Mathematics and Physics, Lanzhou Jiaotong University, Lanzhou 730070, China. [2]Department of Applied Physics, Lanzhou University of Technology, Lanzhou 730050, China. ✉email: liuzj1024@hotmail.com

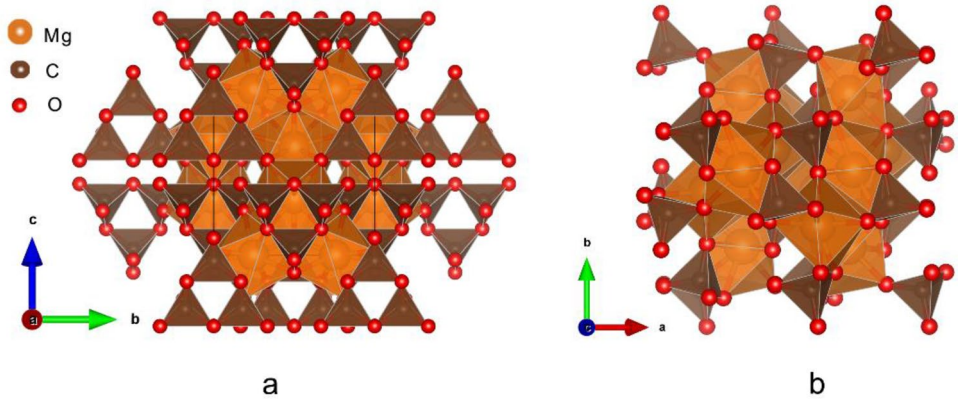


**Figure 1.** Crystal structures of $MgCO_3$-$C2/m$ (**a**) and $Mg_2CO_4$-$P2_1/c$ (**b**) in unit cell. The crystal structures are drawn by VESTA[32].

| Method | a (Å) | b (Å) | c (Å) | $\beta$ | V(Å$^3$) |
|---|---|---|---|---|---|
| **$MgCO_3$-$C2/m$** | | | | | |
| This work | 8.104 | 6.493 | 6.884 | 103.893 | 351.61 |
| Binck et al.[5] | 8.117 | 6.510 | 6.911 | 103.858 | 354.64 |
| **$Mg_2CO_4$-$P2_1/c$** | | | | | |
| This work | 4.383 | 5.358 | 8.293 | 117.56 | 172.65 |
| Gavryushkin et al.[14] | 4.408 | 5.383 | 8.345 | 117.65 | 175.39 |

**Table 1.** Lattice parameters of $MgCO_3$-$C2/m$ and $Mg_2CO_4$-$P2_1/c$ at 110 GPa and 100 GPa, respectively, compared with experimental and previous calculations.

## Methods

First-principles calculations are used to investigate the high-pressure physical properties of $MgCO_3$-$C2/m$ and $Mg_2CO_4$-$P2_1/c$ using projector-augmented wave (PAW)[25] as implemented in VASP[26,27]. The electronic configurations: $2p^63s^2$ for Mg, $2s^22p^2$ for C and $2s^22p^4$ for O are considered for the valence electrons. The Perdew–Burke–Ernzerhof modified solid (PBEsol) in the generalized gradient approximation (GGA)[28] describes the exchange and correlation potentials. The generation of k-point mesh and the calculation of elastic properties utilize the vaspkit program[29]. The cutoff energy for the plane wave is set to 900 eV. The $k$-points mesh of $MgCO_3$-$C2/m$ and $Mg_2CO_4$-$P2_1/c$ are set to $4\times5\times5$ and $13\times9\times7$ using the Monkhorst–Pack scheme[30], respectively. The thermodynamic properties are calculated by the QHA method[31].

## Results and discussion

**Structural parameters, phase transition and equation of state.** The crystal structures of $MgCO_3$-$C2/m$ and $Mg_2CO_4$-$P2_1/c$ in the unit cell are shown in Fig. 1. The optimized lattice parameters are summarized in Table 1 and compared with available experimental and previously calculated results. At 110 GPa, the calculated results of $MgCO_3$-$C2/m$ are consistent with the experimental results[5]. The results for $Mg_2CO_4$-$P2_1/c$ at 100 GPa agree well with the previous calculations[14].

As shown in Fig. 2, the present calculated transition pressure from $Mg_2CO_4$-$Pnma$ to $Mg_2CO_4$-$P2_1/c$ is 44.66 GPa, while Gavryushkin et al. calculated 52 GPa[14]. This error may be caused by the use of different exchange correction functions, PBEsol is used in the present work, while PBE was used by Gavryushkin et al.[14]. The accuracy of using PBEsol to calculate the properties of Mg-carbonate has been examined in the previous studies[13]. In the previous study, $MgCO_3$-$C2/m$ was stable in the lower mantle above 80 GPa[3,5–13,33]. Therefore, in order to facilitate comparison, the high-pressure properties of $MgCO_3$-$C2/m$ and $Mg_2CO_4$-$P2_1/c$ in the pressure range of 50–140 GPa are investigated in this work.

The equations of state for $MgCO_3$-$C2/m$ and $Mg_2CO_4$-$P2_1/c$ at 50 to 140 GPa are shown in Fig. 3. It is found that the equation of state of $MgCO_3$-$C2/m$ is in good agreement with available experimental data[6]. The equation of state of $Mg_2CO_4$-$P2_1/c$ is smaller than that of $MgCO_3$-$C2/m$, and is almost parallel. The formula unit volume of $MgCO_3$-$C2/m$ is smaller than that of $Mg_2CO_4$-$P2_1/c$, which is in line with their molecular formula composition relationship.

**Elastic properties.** For monoclinic $MgCO_3$-$C2/m$ and $Mg_2CO_4$-$P2_1/c$, there are 13 independent elastic constants ($c_{11}$, $c_{12}$, $c_{13}$, $c_{15}$, $c_{22}$, $c_{23}$, $c_{23}$, $c_{25}$, $c_{33}$, $c_{35}$, $c_{44}$, $c_{46}$, $c_{55}$ and $c_{66}$). The elastic constants are calculated using the stress–strain method[29]. In this work, all calculated elastic stiffness constants $c_{ij}$ are checked using the mechanical

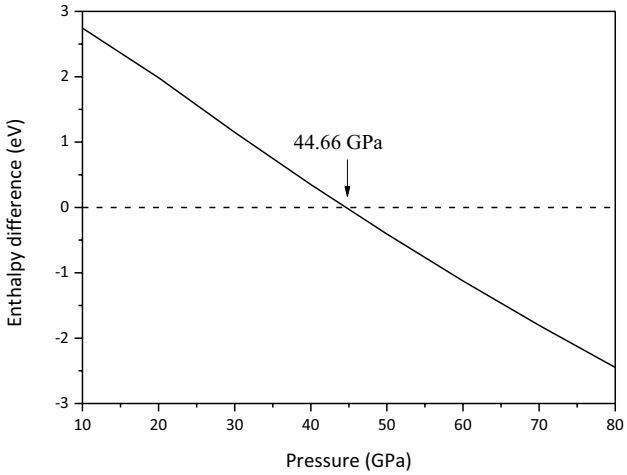


**Figure 2.** Enthalpy difference between $Mg_2CO_4$-$P2_1/c$ and $Mg_2CO_4$-*Pnma*.

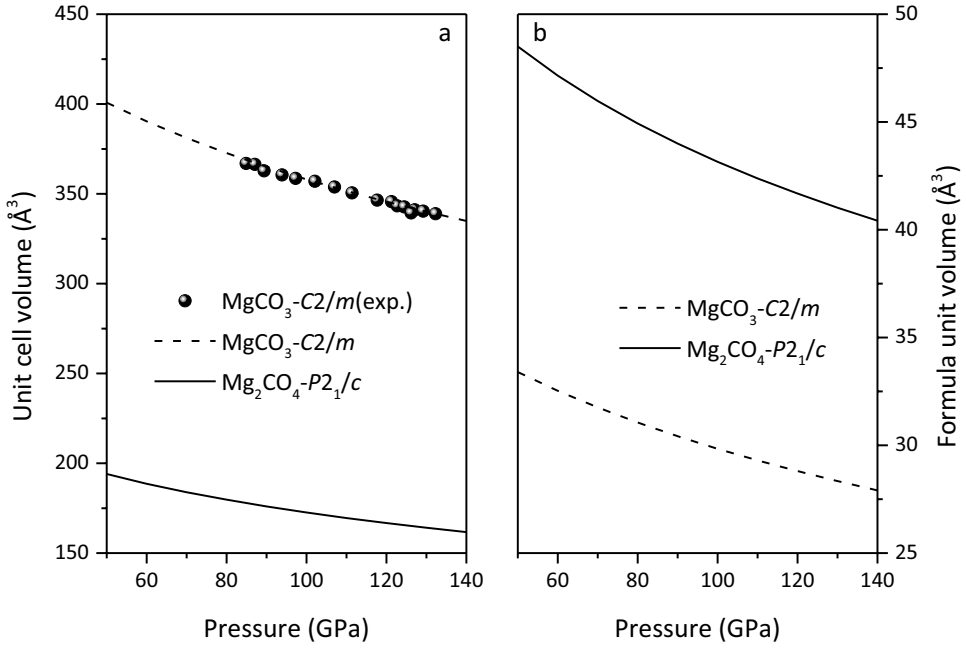


**Figure 3.** Equation of state for $MgCO_3$-$C2/m$ and $Mg_2CO_4$-$P2_1/c$.

stability criteria[34] and find that they all meet the mechanical stability criteria in the studied pressure range, thus they are mechanically stable.

The elastic constants of $MgCO_3$-$C2/m$ and $Mg_2CO_4$-$P2_1/c$ are plotted in Figs. 4 and 5, respectively. It is found from Fig. 4 that at 50–110 GPa, $c_{22} > c_{33} > c_{11}$, indicating that the a-axis of $MgCO_3$-$C2/m$ is the most easily compressed, and the b-axis is the least compressed. At > 110 GPa, $c_{33} > c_{22} > c_{11}$, the c-axis is least likely to be compressed. From Fig. 5, it can be seen that $c_{22} > c_{11} > c_{33}$ in the studied pressure range, indicating that the c-axis of $Mg_2CO_4$-$P2_1/c$ is the most easily compressed, and the b-axis is the least compressible. In the previous study[13], the elastic constants of $MgCO_3$-$R\bar{3}c$ are consistent with the experimental results[21]. Therefore, the predicted elastic constants of $MgCO_3$-$C2/m$ and $Mg_2CO_4$-$P2_1/c$ in this work should be correct, but it needs to be further verified by experiments.

Based on the calculated elastic constants, the bulk modulus $B$ and shear modulus $G$ of $MgCO_3$-$C2/m$ and $Mg_2CO_4$-$P2_1/c$ are calculated using the Voigt-Reuss-Hill method[35–37]. As shown in Fig. 6, the bulk modulus $B$ and shear modulus $G$ of $MgCO_3$-$C2/m$ and $Mg_2CO_4$-$P2_1/c$ increase with increasing pressure, and the bulk modulus $B$ and shear modulus $G$ of $MgCO_3$-$C2/m$ are larger than those of $Mg_2CO_4$-$P2_1/c$ at 50–140 GPa.

**Seismic properties.** Based on the calculated bulk and shear moduli and density, the compression ($V_P$) and shear ($V_S$) velocities of $MgCO_3$-$C2/m$ and $Mg_2CO_4$-$P2_1/c$ are given by the following expressions[38]:

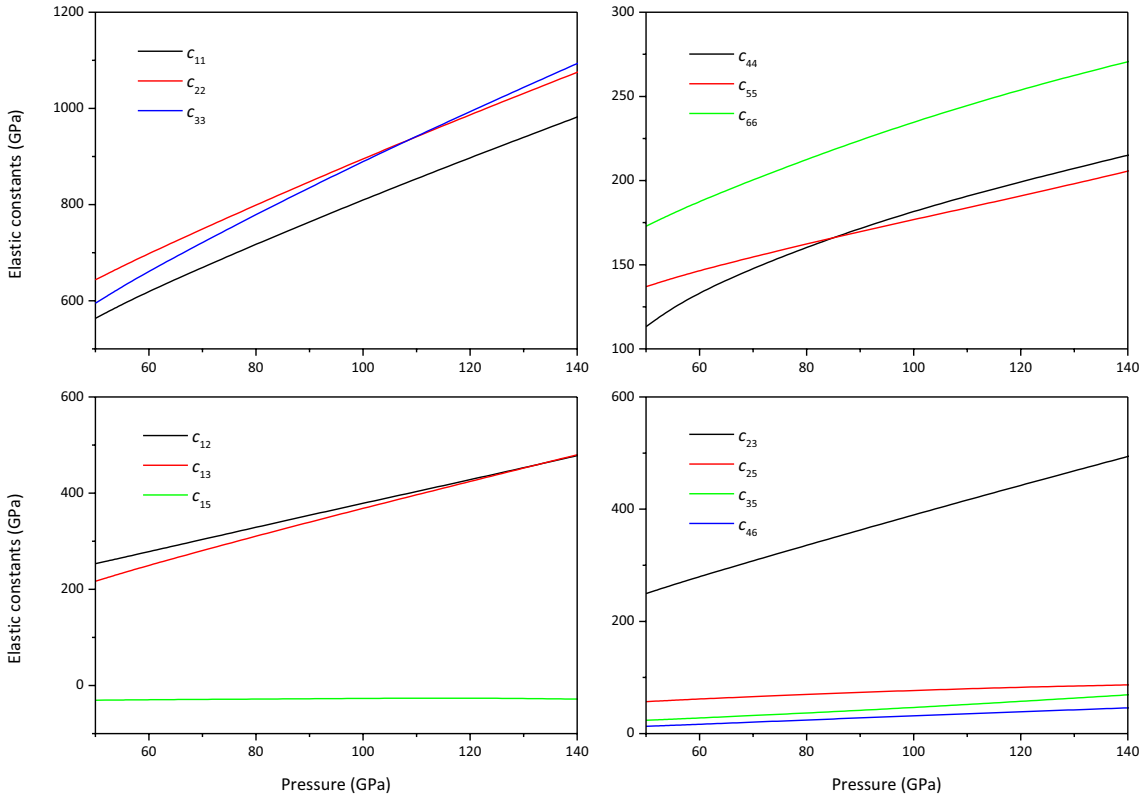


**Figure 4.** Elastic constants of $MgCO_3$-C2/*m*.

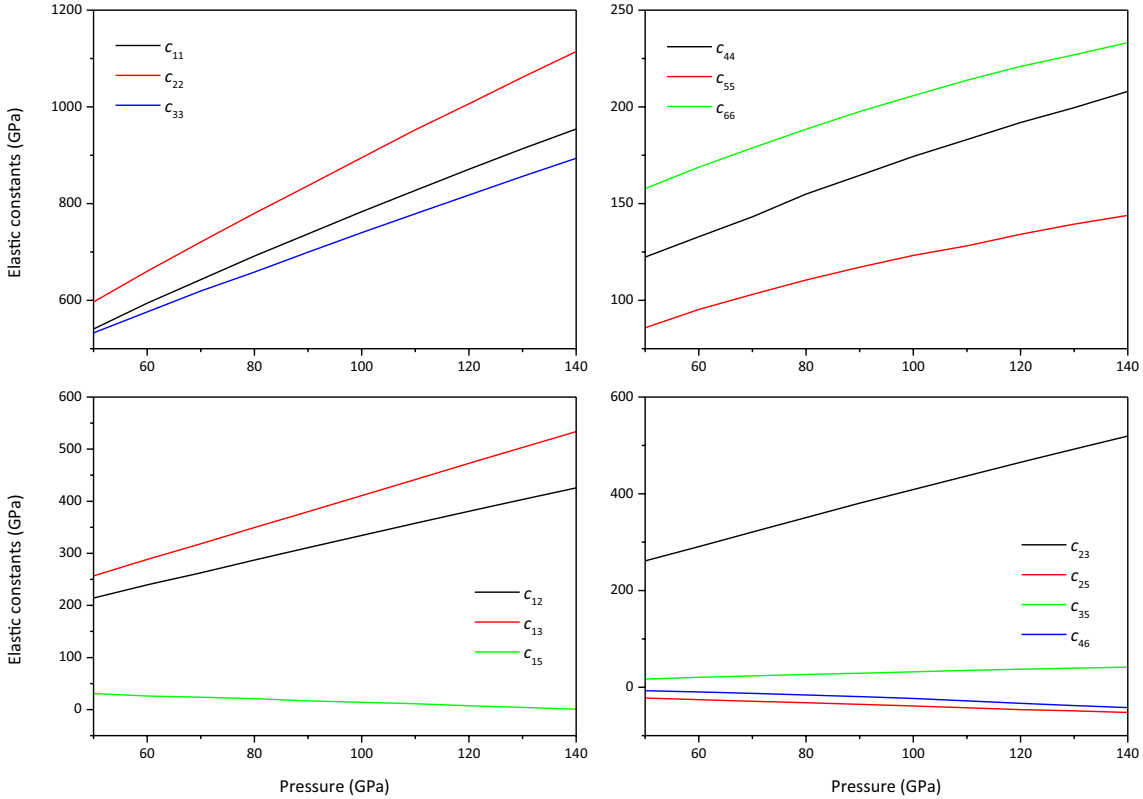


**Figure 5.** Elastic constants of $Mg_2CO_4$-$P2_1/c$.

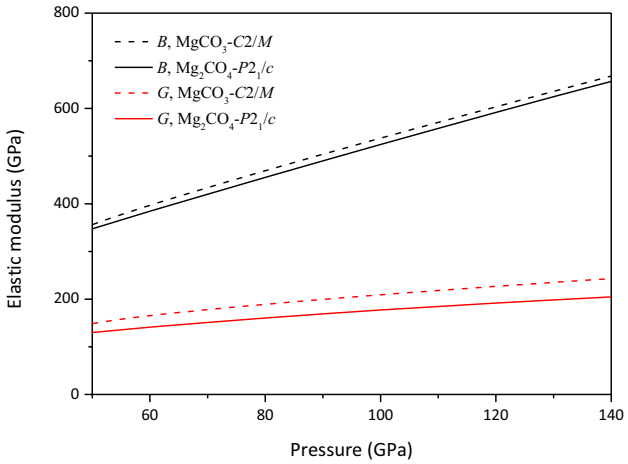


**Figure 6.** Bulk modulus $B$ and shear modulus $G$ of $MgCO_3$-$C2/m$ and $Mg_2CO_4$-$P2_1/c$.

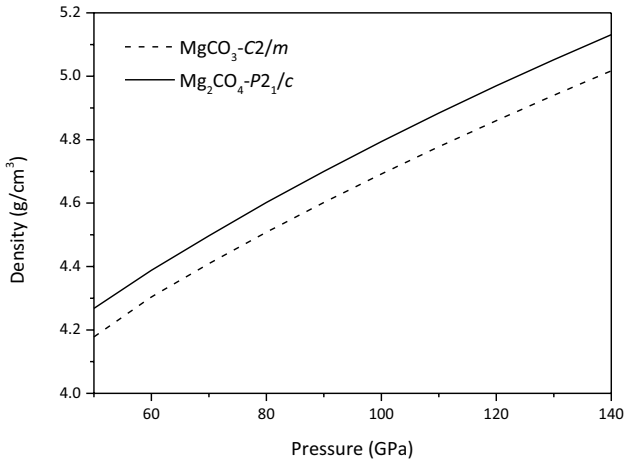


**Figure 7.** Density of $MgCO_3$-$C2/m$ and $Mg_2CO_4$-$P2_1/c$.

$$V_P = \sqrt{\frac{3B + 4G}{3\rho}} \tag{1}$$

$$V_S = \sqrt{\frac{G}{\rho}} \tag{2}$$

As shown in Fig. 7, the density of $Mg_2CO_4$-$P2_1/c$ is larger than that of $MgCO_3$-$C2/m$, and the difference between their bulk modulus and shear modulus is smaller, respectively. Therefore, the $V_P$ and $V_S$ of $MgCO_3$-$C2/m$ are larger than those of $Mg_2CO_4$-$P2_1/c$ in the studied pressure range, and their $V_P$ and $V_S$ tend to be parallel, respectively (See Fig. 8).

The $V_P$ and $V_S$ of $MgCO_3$-$C2/m$ and $Mg_2CO_4$-$P2_1/c$ along different directions can be obtained by solving the Christoffel equation[39] $\left|C_{ijkl}n_jn_l - \rho V^2\delta_{ik}\right| = 0$. In order to visualize the propagation wave velocities of $MgCO_3$-$C2/m$ and $Mg_2CO_4$-$P2_1/c$ along different directions, the AWESoMe program[40,41] is used to plot their 3D representations of $V_P$ and $V_S$ and shear wave splitting and polarization vectors at various pressures (Figs. 9 and 10).

The anisotropy $A_P$ of the $V_P$ for $MgCO_3$-$C2/m$ and $Mg_2CO_4$-$P2_1/c$ is defined as[42]:

$$A_P = \frac{V_{P,\max} - V_{P,\min}}{V_{P,aggregate}} \times 100\%. \tag{3}$$

The polarization anisotropy $A_S$ of the $V_S$ is defined as

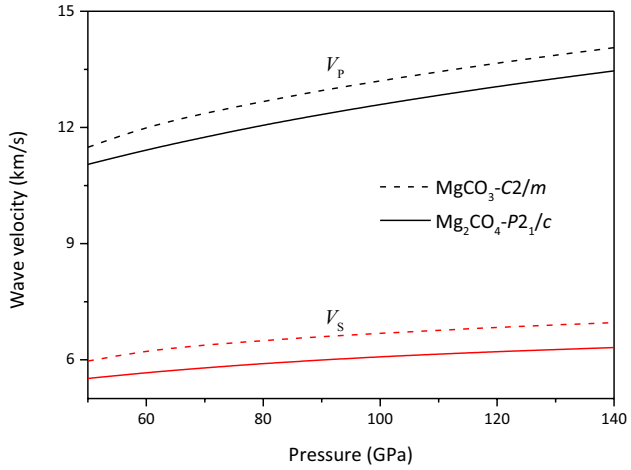


**Figure 8.** Compression ($V_P$) and shear ($V_S$) velocities of $MgCO_3$-$C2/m$ and $Mg_2CO_4$-$P2_1/c$.

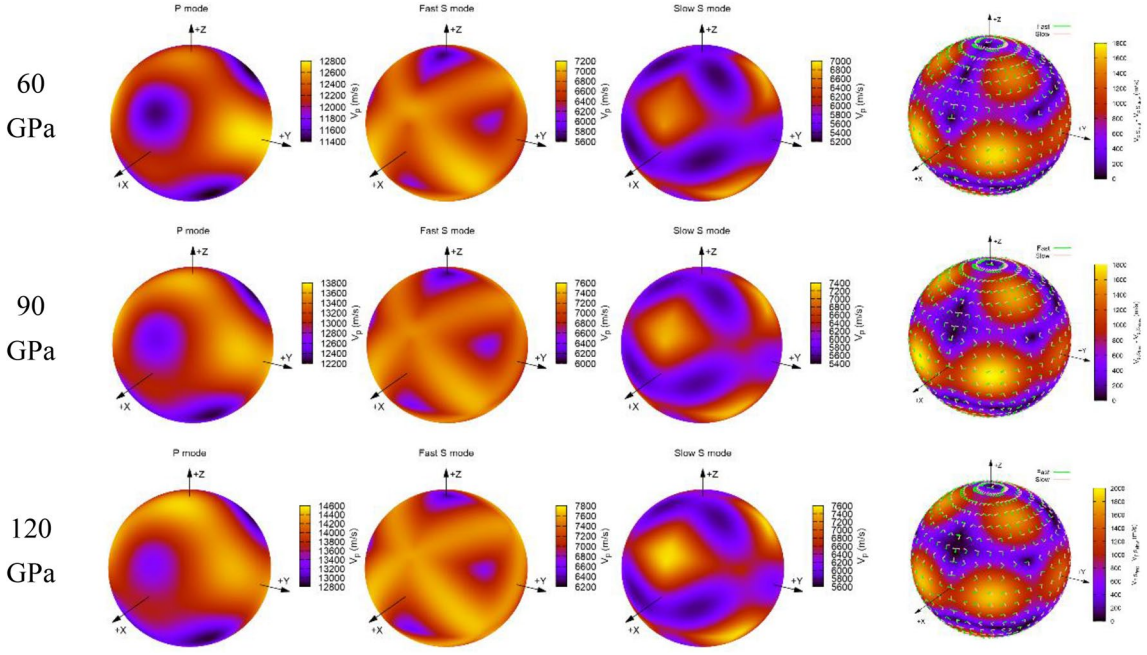


**Figure 9.** 3D representation of the $V_P$ and $V_S$ and the shear wave splitting and polarization vectors of $MgCO_3$-$C2/m$ at various pressures.

$$A_S = \frac{(V_{S1} - V_{S2})_{\max}}{V_{S,aggregate}} \times 100\%. \tag{4}$$

The seismic anisotropies of $MgCO_3$-$C2/m$ and $Mg_2CO_4$-$P2_1/c$ are shown in Fig. 11. The seismic anisotropy of $MgCO_3$-$C2/m$ at 75 GPa is found to be in good agreement with the previous theoretical calculations[10]. The anisotropy of $Mg_2CO_4$-$P2_1/c$ is obviously larger than that of $MgCO_3$-$C2/m$. The seismic anisotropy of $MgCO_3$-$C2/m$ and $Mg_2CO_4$-$P2_1/c$ showed obvious nonlinear dependence on pressure. This is mainly due to the nonlinear pressure of wave velocity caused by the nonlinear pressure dependence of the elastic moduli of $MgCO_3$-$C2/m$ and $Mg_2CO_4$-$P2_1/c$, especially their shear moduli.

Although the previous experimental[4–6] and theoretical[7–13] studies obtained $MgCO_3$-$C2/m$ at high temperature and pressure, they did not consider the reaction with MgO, the main mineral of the Earth's lower mantle. The theoretical[14] and experimental[15] results of Gavryushkin et al. show that $MgCO_3$ reacts with MgO to form $Mg_2CO_4$-$P2_1/c$ orthocarbonate under the temperature and pressure conditions of the lower mantle. By comparing the high-pressure physical properties of $MgCO_3$-$C2/m$ and $Mg_2CO_4$-$P2_1/c$, it is found that their seismic anisotropy is quite different, while the equation of state, elastic modulus, density and wave velocity have similar relationship with pressure. The low wave velocities of $Mg_2CO_4$-$P2_1/c$ are more suitable to explain the existence

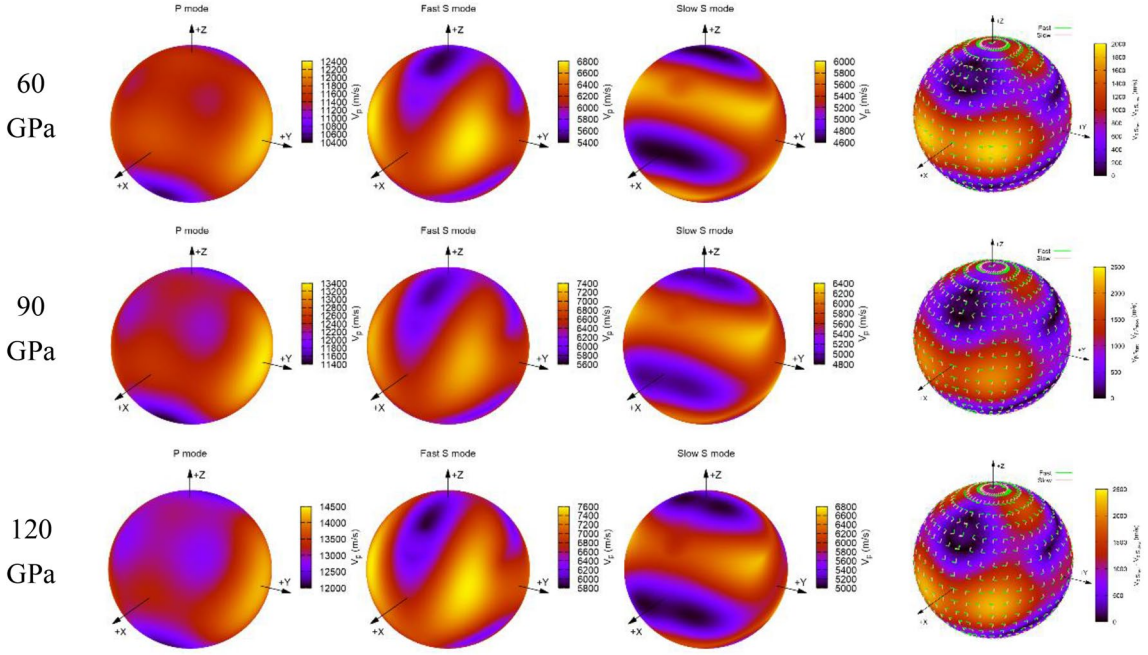


**Figure 10.** 3D representation of the $V_P$ and $V_S$ and the shear wave splitting and polarization vectors of $Mg_2CO_4$-$P2_1/c$ at various pressures.

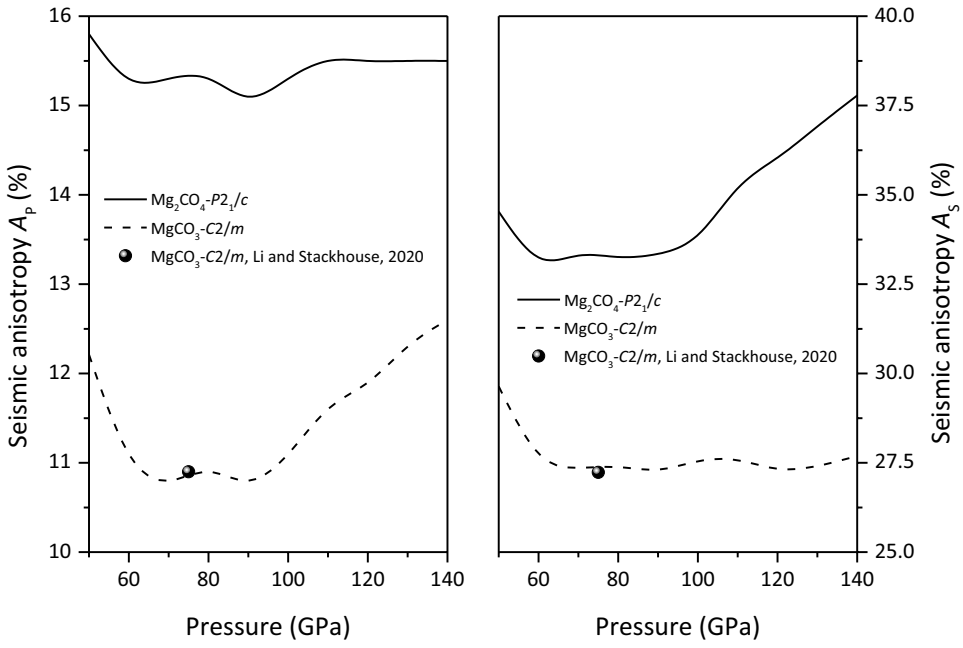


**Figure 11.** Seismic anisotropy of $MgCO_3$-$C2/m$ and $Mg_2CO_4$-$P2_1/c$.

of low-velocity zone near the subducting slab. Therefore, we believe that $Mg_2CO_4$-$P2_1/c$ may exist in the deep mantle, providing strong evidence for carbon storage in carbonate minerals, which may be the main reason why carbonate rocks cannot be detected in the lower mantle.

**Minimum thermal conductivity.** The thermal conductivity of minerals is critical to understanding the Earth's thermal balance and history[43]. The minimum thermal conductivity of $MgCO_3$-$C2/m$ and $Mg_2CO_4$-$P2_1/c$ are calculated using Cahill's model:

$$K_{\min} = (k_B/2.48)n^{2/3}(v_P + 2v_S) \quad (5)$$

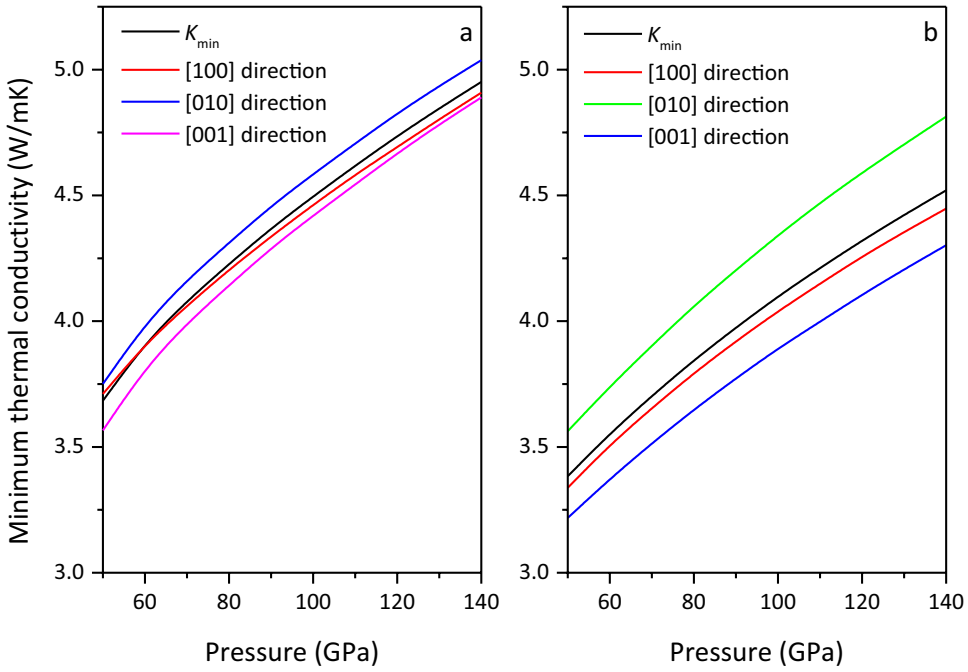


**Figure 12.** Minimum thermal conductivity of $MgCO_3$-$C2/m$ (**a**) and $Mg_2CO_4$-$P2_1/c$ (**b**).

The anisotropy of the minimum thermal conductivity can be calculated by changing Eq. (5) into the following form:

$$K_{min} = (k_B/2.48)n^{2/3}(v_P + v_{S1} + v_{S2}) \tag{6}$$

where $k_B$ is Boltzmann's constant, $n$ is the atomic number density per unit volume. The minimum thermal conductivities of $MgCO_3$-$C2/m$ and $Mg_2CO_4$-$P2_1/c$ are shown in Fig. 12, and it is found that their minimum thermal conductivities increase with the increase of pressure, and that of $MgCO_3$-$C2/m$ is larger than that of $Mg_2CO_4$-$P2_1/c$. In the studied pressure range, $K_{min}[010] > K_{min}[100] > K_{min}[001]$, indicating that the thermal conductivity in the [010] direction is the largest and the thermal conductivity in the [001] direction is the smallest.

**Thermodynamic properties.** Thermodynamic parameters are the preconditions for deriving the thermal state of the Earth's interior. Therefore, the thermodynamic properties of $MgCO_3$-$C2/m$ and $Mg_2CO_4$-$P2_1/c$ are crucial for studying the thermal state of the lower mantle. The constant volume heat capacity ($C_V$) and the thermal expansion coefficient ($\alpha$) of $MgCO_3$-$C2/m$ and $Mg_2CO_4$-$P2_1/c$ at various pressures are depicted in Figs. 13 and 14, respectively. The $C_V$ and $\alpha$ of $MgCO_3$-$C2/m$ are larger than those of $Mg_2CO_4$-$P2_1/c$ under the same pressure.

## Conclusions

On the basis of verifying the structure and equation of state of $MgCO_3$-$C2/m$, the phase transition pressure of $Mg_2CO_4$-$P2_1/c$ is determined. The high-pressure physical properties of $MgCO_3$-$C2/m$ and $Mg_2CO_4$-$P2_1/c$ at 50–140 GPa are investigated by first-principles calculations. By comparison, it is found that the elastic modulus and wave velocity of $Mg_2CO_4$-$P2_1/c$ are smaller than those of $MgCO_3$-$C2/m$, and the density and seismic anisotropy are larger than those of $MgCO_3$-$C2/m$. The low wave velocity of $Mg_2CO_4$-$P2_1/c$ may be more suitable to explain the existence of the low-velocity zone near the subducting slab. Therefore, it is believed that $Mg_2CO_4$-$P2_1/c$ may exist in the deep mantle, providing strong evidence for carbon storage in carbonates and the reason why it cannot be detected in the lower mantle. The minimum thermal conductivity of $MgCO_3$-$C2/m$ is greater than that of $Mg_2CO_4$-$P2_1/c$, and their minimum thermal conductivity is the largest in the [010] direction and the smallest in the [001] direction. The constant volume heat capacity $C_V$ and thermal expansion coefficient $\alpha$ of $MgCO_3$-$C2/m$ are larger than those of $Mg_2CO_4$-$P2_1/c$. Unfortunately, there are no experimental data on the elastic constants, thermodynamic parameters, and minimum thermal conductivity of $MgCO_3$-$C2/m$ and $Mg_2CO_4$-$P2_1/c$, so further verification is required.

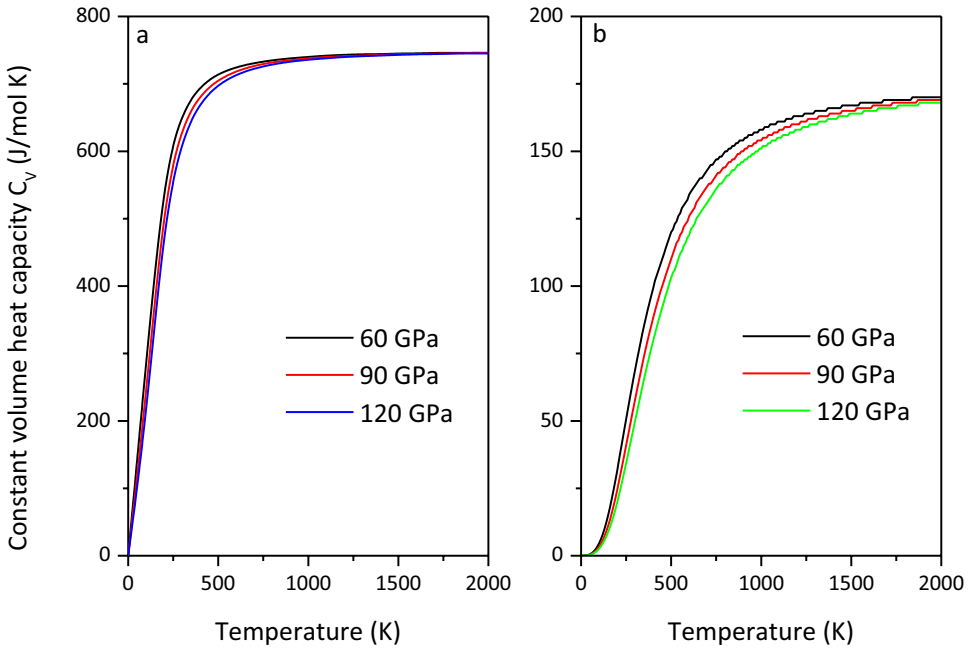


**Figure 13.** Constant volume heat capacity $C_V$ of $MgCO_3$-$C2/m$ (**a**) and $Mg_2CO_4$-$P2_1/c$ (**b**).

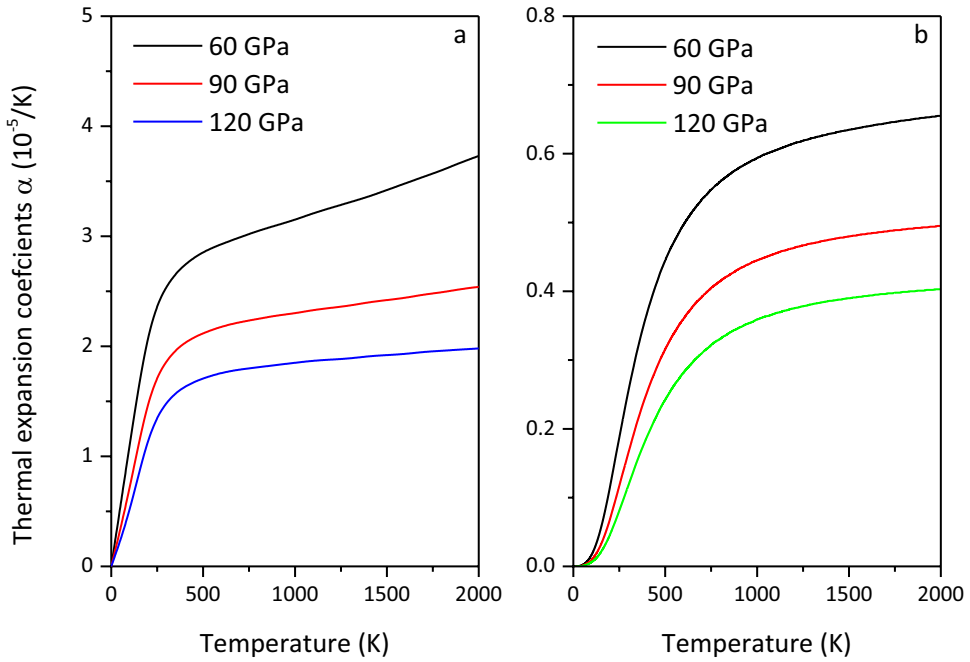


**Figure 14.** Thermal expansion coefficient $\alpha$ of $MgCO_3$-$C2/m$ (**a**) and $Mg_2CO_4$-$P2_1/c$ (**b**).

## Data availability

The datasets used and/or analysed during the current study available from the corresponding author on reasonable request.

Received: 11 October 2022; Accepted: 9 November 2022
Published online: 14 November 2022

## References

1. Isshiki, M. *et al.* Stability of magnesite and its high-pressure form in the lowermost mantle. *Nature* **427**, 60–63 (2004).
2. Plank, T. & Manning, C. E. Subducting carbon. *Nature* **574**, 343–352 (2019).

3. Oganov, A. R., Ono, S., Ma, Y., Glass, C. W. & Garcia, A. Novel high-pressure structures of $MgCO_3$, $CaCO_3$ and $CO_2$ and their role in Earth's lower mantle. *Earth Planet. Sci. Lett.* **273**, 38–47 (2008).
4. Boulard, E. *et al.* New host for carbon in the deep Earth. *Proc. Natl. Acad. Sci. USA.* **108**, 5184–5187 (2011).
5. Binck, J. *et al.* Phase stabilities of $MgCO_3$ and $MgCO_3$-II studied by Raman spectroscopy, X-ray diffraction, and density functional theory calculations. *Phys. Rev. Mater.* **4**, 055001 (2020).
6. Maeda, F. *et al.* Diamond formation in the deep lower mantle: A high-pressure reaction of $MgCO_3$ and $SiO_2$. *Sci. Rep.* **7**, 40602 (2017).
7. Pickard, C. J. & Needs, R. J. Structures and stability of calcium and magnesium carbonates at mantle pressures. *Phys. Rev. B* **91**, 104101 (2015).
8. Marcondes, M. L., Justo, J. F. & Assali, L. V. C. Carbonates at high pressures: Possible carriers for deep carbon reservoirs in the Earth's lower mantle. *Phys. Rev. B* **94**, 104112 (2016).
9. Santos, S. S. M., Marcondes, M. L., Justo, J. F. & Assali, L. V. C. Stability of calcium and magnesium carbonates at Earth's lower mantle thermodynamic conditions. *Earth Planet. Sci. Lett.* **506**, 1–7 (2019).
10. Li, Z. & Stackhouse, S. Iron-rich carbonates stabilized by magnetic entropy at lower mantle conditions. *Earth Planet. Sci. Lett.* **531**, 115959 (2020).
11. Tsuchiya, J., Nishida, R. & Tsuchiya, T. First Principles calculation of the stability of Iron bearing carbonates at high pressure conditions. *Minerals* **10**, 54 (2020).
12. Sagatova, D. N., Shatskiy, A. F., Gavryushkin, P. N., Sagatov, N. E. & Litasov, K. D. Stability of $Ca_2CO_4$-Pnma against the main mantle minerals from ab initio computations. *ACS Earth Space Chem.* **5**, 1709–1715 (2021).
13. Liu, Z. J. *et al.* First-principles calculations of high-pressure physical properties anisotropy for magnesite. *Sci. Rep.* **12**, 3691 (2022).
14. Gavryushkin, P. N., Sagatova, D. N., Sagatov, N. & Litasov, K. D. Formation of Mg-orthocarbonate through the reaction $MgCO_3$+MgO=$Mg_2CO_4$ at Earth's lower mantle P-T Conditions. *Cryst. Growth Des.* **21**, 2986–2992 (2021).
15. Gavryushkin, P. N. *et al.* High-pressure synthesis and ambient-pressure TEM investigation of Mg-orthocarbonate. *Lithos*. https://doi.org/10.2139/ssrn.3966096 (2021).
16. Yamnova, N. A., Zubkova, N. V., Eremin, N. N., Zadov, A. E. & Gazeev, V. M. Crystal structure of larnite β-$Ca_2SiO_4$ and specific features of polymorphic transitions in dicalcium orthosilicate. *Crystallogr. Rep.* **56**, 210–220 (2011).
17. Fyfe, W. S. Lattice energies, phase transformations and volatiles in the mantle. *Phys. Earth Planet. Inter.* **3**, 196–200 (1970).
18. Irving, A. J. & Wyllie, P. J. Melting relationships in CaO-$CO_2$ and MgO-$CO_2$ to 36 kilobars with comments on $CO_2$ in the mantle. *Earth Planet. Sci. Lett.* **20**, 220–225 (1973).
19. Newton, R. C. & Sharp, W. E. Stability of forsterite+$CO_2$ and its bearing on the role of $CO_2$ in the mantle. *Earth Planet. Sci. Lett.* **26**, 239–244 (1975).
20. Katsura, T. *et al.* Stability of magnesite under the lower mantle conditions. *Proc. Japan Acad. Ser. B.* **67**, 57–60 (1991).
21. Yang, J., Mao, Z., Lin, J. F. & Prakapenka, V. B. Single-crystal elasticity of the deep-mantle magnesite at high pressure and temperature. *Earth Planet. Sci. Lett.* **392**, 292–299 (2014).
22. Litasov, K. D., Fei, Y., Ohtani, E., Kuribayashi, T. & Funakoshi, K. Thermal equation of state of magnesite to 32 GPa and 2073 K. *Phys. Earth Planet. Int.* **168**, 191–203 (2008).
23. Matas, J., Gillet, P., Ricard, Y. & Martinez, I. Thermodynamic properties of carbonates at high pressures from vibrational modelling. *Eur. J. Mineral.* **12**, 703–720 (2000).
24. Zhang, J., Martinez, I., Guyot, F., Gillet, P. & Saxena, S. K. X-ray diffraction study of magnesite at high-pressure and high-temperature. *Phys. Chem. Miner.* **24**, 122–130 (1997).
25. Kresse, G. & Joubert, D. From ultrasoft pseudopotentials to the projector augmented-wave method. *Phys. Rev. B* **59**, 1758–1775 (1999).
26. Kresse, G. & Furthmüller, J. Efficiency of ab-initio total enery calculations for metals and semiconductors using a plane-wave basis set. *Comput. Mater. Sci.* **6**, 15–50 (1996).
27. Kresse, G. & Furthmüller, J. Efficient iterative schemes for ab initio total-energy calculations using a plane-wave basis set. *Phys. Rev. B* **54**, 11169–11186 (1996).
28. Perdew, J. P. *et al.* Restoring the density-gradient expansion for exchange in solids and surfaces. *Phys. Rev. Lett.* **100**, 136406 (2008).
29. Wang, V., Xu, N., Liu, J. C., Tang, G. & Geng, W. T. VASPKIT: A user-friendly interface facilitating high-throughput computing and analysis using VASP code. *Comput. Phys. Commun.* **267**, 108033 (2021).
30. Monkhorst, H. J. & Pack, J. D. Special points for Brillouin-zone integrations. *Phys. Rev. B* **13**, 5188–5192 (1976).
31. Otero-de-la-Roza, A., Abbasi-Pérez, D. & Luaña, V. Gibbs2: A new version of the quasiharmonic model code. II. Models for solid-state thermodynamics, features and implementation. *Comput. Phys. Commun.* **182**, 2232–2248 (2011).
32. Momma, K. & Izumi, F. VESTA 3 for three-dimensional visualization of crystal, volumetric and morphology data. *J. Appl. Crystallogr.* **44**, 1272–1276 (2011).
33. Zhao, C. S., Lv, C. J., Xu, L. X., Liang, L. & Liu, J. Raman signatures of the distortion and stability of $MgCO_3$ to 75 GPa. *Am. Mineral.* **106**, 367–373 (2021).
34. Wu, Z.-J. *et al.* Crystal structures and elastic properties of superhard $IrN_2$ and $IrN_3$ from first principles. *Phys. Rev. B* **76**, 054115 (2007).
35 Hill, R. The elastic behavior of a crystalline aggregate. *Proc. Phys. Soc. Lond.* **65A**, 349–354 (1952).
36. Voigt, W. *Lehrbuch der Kristallphysik-mit Ausschluß der Kristalloptik* (Vieweg+Teubner Verlag, 1966).
37. Reuss, A. Calulation of yielding mixed crystals plasticity condition for single crystals. *Z. Angew. Math. Mech.* **9**, 49–58 (1929).
38. Anderson, O. L. A simplified method for calculating the debye temperature from elastic constants. *J. Phys. Chem. Solids* **24**, 909–917 (1963).
39. Anderson, D. L. *Theory of the Earth* (Blackwell Scientific Publications, 1989).
40. Muñoz-Santiburcio, D., Hernández-Laguna, A. & Soto, J. I. AWESoMe: A code for the calculation of phase and group velocities of acoustic waves in homogeneous solids. *Comput. Phys. Commun.* **192**, 272–277 (2015).
41. Muñoz-Santiburcio, D. & Hernández-Laguna, A. AWESoMe 1.1: A code for the calculation of phase and group velocities of acoustic waves in homogeneous solids. *Comput. Phys. Commun.* **217**, 212–214 (2017).
42. Kiefer, B., Stixrude, L., Hafner, J. & Kresse, G. Structure and elasticity of wadsleyite at high pressures. *Am. Mineral.* **86**, 1387–1395 (2001).
43. Zhou, Y., Dong, Z. Y., Hsieh, W. P., Goncharov, A. F. & Chen, X. J. Thermal conductivity of materials under pressure. *Nat. Rev. Phys.* **4**, 319–335 (2022).


## Acknowledgements

This work is supported by the Industrial Support and Guidance Project of Colleges and Universities of Gansu Province (No. 2022CYZC-37), the Key Natural Science Foundation of Gansu Province (No. 20JR5RA211) and the Talent Innovation and Entrepreneurship Project of Lanzhou City (No. 2020-RC-18).

## Author contributions

Z.-J.L. designed the calculations and wrote the manuscript. X.-W.S. and C.-R.Z. analyzed the results. J.-Q.J. and T.L. performed partial calculations. All authors reviewed the manuscript.

## Competing interests

The authors declare no competing interests.

## Additional information

**Correspondence** and requests for materials should be addressed to Z.-J.L.

**Reprints and permissions information** is available at www.nature.com/reprints.

**Publisher's note** Springer Nature remains neutral with regard to jurisdictional claims in published maps and institutional affiliations.